

Fast Equivariant Imaging: Acceleration for Unsupervised Learning via Augmented Lagrangian and Auxiliary PnP Denoisers

Guixian Xu

*School of Mathematics,
University of Birmingham*

GXX422@STUDENT.BHAM.AC.UK

Jinglai Li

*School of Mathematics,
University of Birmingham*

J.LI.10@BHAM.AC.UK

Junqi Tang

*School of Mathematics,
University of Birmingham*

J.TANG.2@BHAM.AC.UK

Abstract

In this work, we propose Fast Equivariant Imaging (FEI), a novel unsupervised learning framework to rapidly and efficiently train deep imaging networks without ground-truth data. From the perspective of reformulating the Equivariant Imaging based optimization problem via the method of Lagrange multipliers and utilizing plug-and-play denoisers, this novel unsupervised scheme shows superior efficiency and performance compared to the vanilla Equivariant Imaging paradigm. In particular, our FEI schemes achieve an order-of-magnitude (10x) acceleration over standard EI on training U-Net for X-ray CT reconstruction and image inpainting, with improved generalization performance.

1. Introduction

In this work, we consider unsupervised learning of deep neural networks for solving inverse problems of the form:

$$y \approx Ax^\dagger, \quad (1)$$

with reference signal / image $x^\dagger \in \mathbb{R}^n$ to be estimated, noisy measurements $y \in \mathbb{R}^m$. $A \in \mathbb{R}^{m \times n}$ is the forward operator potentially with $m \ll n$, and can be a downsampling operator for super-resolution task, masks for inpainting, Gaussian linear measurements for compressive sensing, Radon transform for CT/PET, to name a few. In this setting, one can construct an MAP estimator for x^\dagger by solving the following optimization problem:

$$x^* = \arg \min_x \{f_{\text{mc}}(Ax, y) + R(x)\}, \quad (2)$$

where $f_{\text{mc}}(Ax, y)$ is the measurement consistency (MC) term such as ℓ_1 loss, ℓ_2 loss and SURE-loss (Chen et al., 2022), $R(x)$ is the prior or regularizer. The paradigm presented in this paper could be easily extended to handle different types of noise (e.g., Poisson, Gamma, mixed Poisson-Gamma, or other models). This

should be done by replacing f_{mc} by the minus log-likelihood of the appropriate distribution, as done in [Chen et al. \(2022\)](#).

1.1 Equivariant Imaging

In unsupervised learning, since we only have access to noisy measurements \mathcal{Y} , one can reconstruct the signal/image by learning a reconstruction function $G_\theta : \mathbb{R}^m \rightarrow \mathbb{R}^n$ such that $G_\theta(y) \approx x^\dagger$. By enforcing that the inverse mapping G_θ is consistent in the measurement domain, the following measurement consistence estimator (MC) can be obtained,

$$\min_{\theta} \mathbb{E}_{y \in \mathcal{Y}} f_{\text{mc}}(AG_\theta(y), y). \quad (\text{MC})$$

However, the MC constraint is not enough to learn the inverse mapping, as it cannot capture information about the signal/image outside the range of the operator A^\top , as explained in [Chen et al. \(2021\)](#).

In order to learn beyond the range space of A^\top , [Chen et al. \(2021\)](#) takes advantage of some mild prior information mainly about the symmetries of plausible signal/image, *i.e.*, signal/image is invariant to certain groups of transformations, such as shifts, rotations, reflections, etc. According to invariance, composition $G_\theta \circ A$ should be equivariant to the transformation T_g , *i.e.*

$$G_\theta(AT_g x) = T_g G_\theta(Ax) \quad (3)$$

where $T_g \in \mathbb{R}^{n \times n}$ are unitary matrices. This equivariant regularization leads to the following unsupervised learning paradigm:

$$\min_{\theta} \mathbb{E}_{y \in \mathcal{Y}, g \sim \mathcal{G}} \{f_{\text{mc}}(y, AG_\theta(y)) + \alpha \|T_g G_\theta(y) - G_\theta(AT_g G_\theta(y))\|_2^2\}. \quad (4)$$

This deep-learning-based unsupervised method has recently achieved state-of-the-art performance for a host of inverse problems ([Chen et al., 2021, 2022](#); [Terris et al., 2024](#)). Their success has been attributed to their ability to explore group symmetry from a range of physics, at the cost of cumbersome and time-consuming training. However, one of the main challenges of this type of unsupervised schemes is the computational cost of training due to the slow convergence and large computational complexity across training iterations, particularly for large-scale inverse problems and advanced architectures such as unrolling ([Monga et al., 2021](#); [Zhou et al., 2024](#)). In our recent work of Sketched EI ([Xu et al., 2024](#)) we partially addressed the computational complexity issue for inverse problems on which dimensionality reduction strategies can be applied. In this work, we aim to address the problem of slow convergence of standard optimizers such as Adam ([Kingma and Ba, 2015](#)) to minimize this EI objective.

1.2 Lagrange-based Splitting method

The success of EI in unsupervised learning has created a pressing need to efficiently solve (4), especially for large-scale datasets where computational scalability is critical. In this work, we explore from an optimization perspective to accelerate this promising unsupervised method via alternating minimization ([Afonso et al., 2010](#)), namely Fast Equivariant Imaging (FEI), for faster convergence.

First, it should be mentioned that the objective (4) can be seen as the Lagrangian of constrained optimization problems:

$$\min_{\mathbf{u}, \theta} \mathbb{E}_{y \in \mathcal{Y}, g \sim \mathcal{G}} \{f_{\text{mc}}(y, A\mathbf{u}) + \alpha \|T_g G_\theta(y) - G_\theta(AT_g G_\theta(y))\|_2^2\} \quad \text{subject to} \quad \mathbf{u} = G_\theta(y), \quad (5)$$

The approach proposed in this paper is based on variable splitting ([Afonso et al., 2010](#)). The idea is to split the variables \mathbf{u} and θ , each to serve as the argument for each of the two functions, and then minimize the

sum of the two functions under the constraint that the two variables have to be equal, so that the problems are equivalent. By decoupling the measurement-consistency term as a numerical block explicitly from network complexity, enabling faster and more reliable convergence to optimal.

Our modification is achieved using an Lagrangian formulation of the problem, and is solved using an alternating-direction minimization method. From numerical experiments, we show that this fast EI method and its variant can improve both the convergence rate and the performance.

1.3 Relation to Prior Works

Our method (FEI) is a significantly improved variant of Equivariant Imaging (EI) (Chen et al., 2021, 2022), which is based on the alternating proximal gradient (Driggs et al., 2021; Afonso et al., 2010) optimization. The further PnP-FEI is a combination of the FEI and plug-and-play prior. It combines a pre-trained denoiser with an explicit EI prior and solves the problem by ADMM.

We differ from Chen et al. (2021) in two important ways: First, the way they minimize the objective function is by optimizing the data consistency term and the equivariance term uniformly in a single backpropagation, which hence enjoys moderate convergence and time-consuming training. In contrast, we consider a more aggressive minimization for the data consistency term via proximal alternating minimization. A second crucial difference is that within our FEI scheme, we can easily incorporate plug-and-play framework as implicit priors to further speed the convergence. In sharp contrast, the vanilla EI, by only exploiting group symmetry of the physics, can be seen as a special case of our proposed PnP-FEI. Although we focus only on accelerating EI in this work, the same algorithmic structure can be easily extended to more recent variants of EI such as Robust Equivariant Imaging (REI) (Chen et al., 2022), Multi-Operator Imaging (MOI) (Tachella et al., 2022), and our recently proposed Sketched Equivariant Imaging (SkEI) (Xu et al., 2024), which utilizes dimensionality reduction techniques for acceleration.

1.4 Contributions

We summarize three major contributions from our work:

- We propose an efficient unsupervised training paradigm FEI which conceptually splits the original brute-force EI training into two alternating steps: a Latent-Reconstruction Step and a Pseudo-Supervision Step. We demonstrate numerically that such a splitting can massively accelerate the unsupervised training of deep imaging networks.
- Under the FEI splitting framework, we propose two novel optimization schemes for efficiently implementing FEI, based on a new integration of adaptive gradient methods (such as Adam) with Half-Quadratic Splitting and Linearized ADMM. We utilize the gradient history of the subproblems from previous HQS/ADMM iterations to update the network parameters to ensure the fastest possible convergence.
- Building upon FEI, we also propose the first unsupervised training scheme PnP-FEI which utilizes pretrained denoisers for further numerical improvements. Thanks to the splitting provided by FEI, we can effectively utilize pretrained image-domain priors such as deep denoiser within our framework, in the Pseudo-Supervision Step. This is the first paradigm which utilizes both the primal domain (image) prior and the dual domain (measurement) prior for unsupervised training of deep imaging networks.

2. Proposed Methods

In this section, we present our FEI framework which is based on splitting the original objective of EI into two alternating subproblems: Latent-reconstruction and Pseudo-supervision. This leads to two options for FEI algorithmically, one with a style of Half-Quadratic Splitting, and one with a style of Linearized ADMM.

2.1 Fast Equivariant Imaging — Option 1 (Adaptive Half Quadratic Splitting)

We first reformulate (4) by substituting $\mathbf{u} = G_\theta(y)$ as follows

$$\min_{\theta, \mathbf{u}} \mathbb{E}_{y \in \mathcal{Y}, g \sim \mathcal{G}} \{f_{\text{mc}}(y, A\mathbf{u}) + \alpha \|T_g G_\theta(y) - G_\theta(AT_g G_\theta(y))\|_2^2\}, \quad \text{s.t. } \mathbf{u} = G_\theta(y). \quad (6)$$

Typical choices for the measurement consistency term $f_{\text{mc}}(x)$ include ℓ_1 loss, ℓ_2 loss or SURE-loss (Chen et al., 2022), etc. We simply substitute $G_\theta(y)$ with \mathbf{u} in the MC term and further incorporate the EI regularizer. From another perspective, the neural network $G_\theta(y)$ in (4) is replaced by an auxiliary variable \mathbf{u} .

To solve this new problem with the choice of Euclidean norm of f , we first rewrite the Lagrangian with penalty parameter λ ,

$$\mathcal{L}_{\lambda, \alpha}(\mathbf{u}, \theta) = \mathbb{E}_{y \in \mathcal{Y}, g \sim \mathcal{G}} \{f_{\text{mc}}(y, A\mathbf{u}) + \frac{\lambda}{2} \|\mathbf{u} - G_\theta(y)\|_2^2 + \alpha \|T_g G_\theta(y) - G_\theta(AT_g G_\theta(y))\|_2^2\}. \quad (7)$$

We then address problem (7) with half quadratic splitting (HQS) algorithm due to its simplicity. Note that a very large λ will force \mathbf{u} to be approximately equal to $G_\theta(y)$. Usually, λ varies in a non-descending order during the following iterative solution

$$\mathbf{u}_{t+1} \approx \arg \min_{\mathbf{u}} \mathcal{L}_{\lambda, \alpha}(\mathbf{u}, \theta_t); \quad \rightarrow \textit{Latent reconstruction step} \quad (8)$$

$$\theta_{t+1} \approx \arg \min_{\theta} \mathcal{L}_{\lambda, \alpha}(\mathbf{u}_{t+1}, \theta); \quad \rightarrow \textit{Pseudo supervision step} \quad (9)$$

This Lagrangian with respect to \mathbf{u} is convex, which means that the minimization over \mathbf{u} can simply be obtained by first-order gradient descent, so the subproblem (8) is equivalent to the following:

$$\min_{\mathbf{u}} \mathbb{E}_{y \in \mathcal{Y}} \{f_{\text{mc}}(y, A\mathbf{u}) + \frac{\lambda}{2} \|\mathbf{u} - G_\theta(y)\|_2^2\}, \quad (10)$$

we propose solving (10) via Nesterov Accelerated Gradient (NAG) (Nesterov, 1983, 2007), with the details present in Algorithm 2. Of course, one could also use other optimizers, such as stochastic gradient methods (Ehrhardt et al., 2025) (if the objective can be minibatched) or quasi-Newton methods (Tan et al., 2024) for this step.

However, the Lagrangian with respect to θ is nonconvex, which means the minimization over θ is often intractable. Here we bypass it by calling backpropagating over θ and taking one gradient descent step using an adaptive gradient method (Adam by default). The complete algorithm for Lagrangian-based fast equivariant imaging can be found in Algorithm 1. Note that in each iteration we typically just run 1 iteration of Adam for the Pseudo-supervision step, while the gradient and momentum history of Adam is inherited from previous Pseudo-supervision steps.

Algorithm 1 Fast Equivariant Imaging (FEI-Option 1)

1: **Inputs:**

- \mathcal{Y} - Observations (training dataset)
- λ - Lagrangian multiplier
- α - EI regularization parameter
- N - number of epochs
- \mathbf{u}_0 - initial NAG point
- v_0 - initial NAG velocity point
- β - NAG momentum factor
- η - NAG step size
- J - number of NAG iterations
- \mathcal{G} - Group of transformations

2: **Initialize:** Neural network G_θ , $\mathbf{u}_0 = A^\dagger y$, $v_0 = \mathbf{0}$, $k = 0$;

3: **For** $i = 0, \dots, N - 1$ **do:**

4: **For** $y \in \mathcal{Y}$ **do:**

5: Sample T_g where $g \sim \mathcal{G}$;

6: Compute $x_0 = G_{\theta_k}(y)$, $\mathbf{u}_k = x_0$;

7: Set $f(\mathbf{u}) = f_{\text{mc}}(y, A\mathbf{u}) + \frac{\lambda}{2} \|\mathbf{u} - G_{\theta_k}(y)\|_2^2$;

8: Update $\mathbf{u}_{k+1} = \mathcal{A}(f, J, \mathbf{u}_k, v_k, \beta, \eta)$ via NAG algorithm presented in Algorithm 2;

9: Let $x_1 = \mathbf{u}_{k+1}$;

10: Transform $x_2 = T_g(x_1)$;

11: Compute $x_3 = G_{\theta_k}(Ax_2)$;

12: Update θ_{k+1} via progressively minimizing loss $\mathcal{L} = \mathbb{E}_{g \sim \mathcal{G}} \{\|x_0 - x_1\|_2^2 + \alpha \|x_2 - x_3\|_2^2\}$ using a gradient-based optimizer (such as Adam) in each iteration;

13: $k \leftarrow k + 1$

14: **End For**

15: **End For**

16: **Output:** G_{θ^*}

Algorithm 2 Nesterov Accelerated Gradient (NAG) – $\mathcal{A}(f, J, \mathbf{u}_0, v_0, \beta, \eta)$

1: **Inputs:** Objective function f , number of iterations J , initial point \mathbf{u}_0 , initial velocity point v_0 , momentum factor β , step size η

2: **Output:** Estimated point \mathbf{u}_J ;

3: **For** $j = 0, \dots, J - 1$ **do:**

4: Compute one-step ahead point $\mathbf{u}_{\text{ahead}} = \mathbf{u}_j - \beta v_j$;

5: Compute one-step ahead gradient $\nabla f(\mathbf{u}_{\text{ahead}})$;

6: Compute next velocity $v_{j+1} = \beta v_j + \eta \nabla f(\mathbf{u}_{\text{ahead}})$;

7: Update $\mathbf{u}_{j+1} = \mathbf{u}_j - v_{j+1}$;

8: **End For**

2.2 Fast Equivariant Imaging — Option 2 (Adaptive Linearized ADMM Splitting)

First, starting with (6), we turn the constraint into a penalty using the Augmented Lagrangian (AL) (Afonso et al., 2010),

$$\mathcal{L}_\lambda(\mathbf{u}, \theta, \mathbf{L}) := \mathbb{E}_{y \in \mathcal{Y}, g \in \mathcal{G}} \{f_{\text{mc}}(y, A\mathbf{u}) + \alpha \|T_g G_\theta(y) - G_\theta(AT_g G_\theta(y))\|_2^2 + \langle \mathbf{L}, \mathbf{u} - G_\theta(y) \rangle + \frac{\lambda}{2} \|\mathbf{u} - G_\theta(y)\|_2^2\} \quad (11)$$

for a penalty weight $\lambda > 0$. Applied to (11), every iteration of ADMM would minimize the Augmented Lagrange with respect to \mathbf{u} , then with respect to θ , and then update the dual variable \mathbf{L} , which are presented as follows:

$$\begin{aligned} \mathbf{u}_{k+1} &\in \arg \min_{\mathbf{u}} \mathcal{L}_\lambda(\mathbf{u}, \theta_k, \mathbf{L}_k), \quad \rightarrow \textit{Latent reconstruction step} \\ \theta_{k+1} &\in \arg \min_{\theta} \mathcal{L}_\lambda(\mathbf{u}_{k+1}, \theta, \mathbf{L}_k), \quad \rightarrow \textit{Pseudo supervision step} \\ \mathbf{L}_{k+1} &= \mathbf{L}_k - \tau(\mathbf{u}_{k+1} - G_{\theta_{k+1}}(y)). \end{aligned} \quad (12)$$

then take only one descent step in both \mathbf{u} and θ . Specifically, fixing θ_k, \mathbf{L}_k , the update of \mathbf{u}_{k+1} can be performed by one step gradient descent, then fixing $\mathbf{u}_{k+1}, \mathbf{L}_k$, the update of θ is done by solving

$$\theta_{k+1} = \arg \min_{\theta} \mathbb{E}_{y \in \mathcal{Y}, g \sim \mathcal{G}} \alpha \|T_g G_\theta(y) - G_\theta(AT_g G_\theta(y))\|_2^2 + \frac{\lambda}{2} \|\mathbf{u}_{k+1} - G_\theta(y) - \mathbf{L}_k\|_2^2, \quad (13)$$

which can be updated by calling backpropagating and taking one adaptive gradient descent (Adam by default) step θ . Note that in each iteration we typically just run 1 iteration of Adam for the Pseudo-supervision step, while the gradient and momentum history of Adam is inherited from previous Pseudo-supervision steps. As for the Lagrange multiplier vector \mathbf{L} , its update is much easier, given by

$$\mathbf{L}_{k+1} = \mathbf{L}_k - \tau(\mathbf{u}_{k+1} - G_{\theta_{k+1}}(y)) \quad (14)$$

as emerging from the AL method (Afonso et al., 2010).

2.3 Fast Plug-and-Play Equivariant Imaging

The plug-and-play (Venkatakrishnan et al., 2013) prior is a flexible framework that incorporates state-of-the-art denoising algorithms as priors in more challenging inverse problems. Our goal here is to bring this method to Fast Equivariant Imaging, in the hope of boosting its convergence rate and its performance as well. Using the last two terms of (11), we get the scaled form,

$$\min_{\theta, \mathbf{u}} \mathbb{E}_{y \in \mathcal{Y}, g \sim \mathcal{G}} \{f_{\text{mc}}(y, A\mathbf{u}) + \alpha \|T_g G_\theta(y) - G_\theta(AT_g G_\theta(y))\|_2^2 + \frac{\lambda}{2} \|\mathbf{u} - G_\theta(y) - \mathbf{L}\|_2^2\}. \quad (15)$$

The remedy for this problem comes in the form of ADMM, which amounts to a sequential update of the three unknowns in this expression: θ , \mathbf{u} , and \mathbf{L} . Fixing θ_k, \mathbf{L}_k , \mathbf{u} should be updated by solving

$$\mathbf{u}_{k+1} = \arg \min_{\mathbf{u}} f_{\text{mc}}(y, A\mathbf{u}) + \frac{\lambda}{2} \|\mathbf{u} - G_{\theta_k}(y) - \mathbf{L}_k\|_2^2, \quad (16)$$

this is a strictly convex quadratic function to be minimized, which can be solved exactly (naturally, up to numerical precision) as follows (for the case where ℓ_2 loss is used for MC term):

$$\mathbf{u}_{k+1} = (A^T A + \lambda I)^{-1} \cdot (A^T y + \lambda G_{\theta_k}(y) + \lambda \mathbf{L}_k). \quad (17)$$

Algorithm 3 Fast Equivariant Imaging (FEI-Option 2)

1: **Inputs:**

- \mathcal{Y} - Observations (training dataset)
- \mathbf{L} - Augmented Lagrangian multiplier
- λ - Augmented Lagrangian free parameter
- α - EI regularization parameter
- N - number of epochs
- \mathcal{G} - Group of transformations
- \mathbf{u} - Initial gradient descent point of (18)
- γ - Gradient descent step size

2: **Initialize:** Neural network G_θ , $\mathbf{L}_0 = \mathbf{0}$, $\mathbf{u}_0 = \mathbf{0}$, $k = 0$;3: **For** $i = 0, \dots, N - 1$ do:4: **For** $y \in \mathcal{Y}$ do:5: Sample T_g where $g \sim \mathcal{G}$;6: Compute $x_0 = G_{\theta_k}(y)$, by default let $\mathbf{u}_k = x_0$;7: Update $\mathbf{u}_{k+1} = \mathbf{u}_k - \gamma[\nabla f_{\text{mc}}(y, A\mathbf{u}_k) + \lambda(\mathbf{u}_k - G_{\theta_k}(y) - \mathbf{L}_k^{(y)})]$ 8: Let $x_1 = \mathbf{u}_{k+1}$;9: Transform $x_2 = T_g(x_1)$;10: Compute $x_3 = G_{\theta_k}(Ax_2)$;11: Update θ_{k+1} via progressively minimizing $\mathcal{L} = \mathbb{E}_{g \sim \mathcal{G}}\{\|x_0 + \mathbf{L}_k^{(y)} - x_1\|_2^2 + \alpha\|x_2 - x_3\|_2^2\}$ using an adaptive gradient-based optimizer (such as Adam) in each iteration;12: Update $\mathbf{L}_{k+1}^{(y)} = \mathbf{L}_k^{(y)} - \tau(x_1 - G_{\theta_{k+1}}(y))$;13: $k \leftarrow k + 1$ 14: **End For**15: **End For**16: **Output:** G_{θ^*}

However, solving this linear system exactly often requires enormous computational efforts, which hinders the convergence of the algorithm, and we suggest solving it in one of two ways: The first option is to use the one gradient-descent step strategy as presented in Algorithm 3. An alternative approach to update \mathbf{u} is Plug-and-Play, for the Lagrangian quadratic data-fidelity term (16), the classical PnP algorithm reads

$$\mathbf{u}_{k+1} = \mathcal{D}(\mathbf{u}_k - \eta[\nabla f_{\text{mc}}(y, A\mathbf{u}_k) + \lambda(\mathbf{u}_k - G_{\theta_k}(y) - \mathbf{L}_k)]), \quad (18)$$

where \mathbf{u}_{k+1} is obtained by one step gradient descent and then denoising, and $\mathcal{D}(\cdot)$ represents classical denoisings such as BM3D (Dabov et al., 2007), DnCNN (Zhang et al., 2017), etc. This motivates us to solve (16) in a proximal way and replace the proximal operator with other denoising algorithms, in a similar fashion to Plug-and-Play.

The Algorithm 4 summarizes the steps to be taken to apply this overall algorithm to manage the minimization of the objective of equivariant imaging. Moreover, taking into account the more recent equivariant PnP (Terris et al., 2024; Tang et al., 2024), we can also modify the PnP step with equivariant denoisers. We present this option in Algorithm 5.

Algorithm 4 Fast Equivariant Imaging with Plug-and-Play (PnP-FEI)

1: **Inputs:**

- | | |
|---|---|
| • \mathcal{Y} - Observations (training dataset) | • N - number of epochs |
| • \mathbf{L} - Augmented Lagrangian multiplier | • \mathcal{G} - Group of transformations |
| • λ - Augmented Lagrangian free parameter | • \mathbf{u} - Initial gradient descent point of (18) |
| • $\mathcal{D}(\cdot)$ - Denoiser | • γ - Gradient descent step size in PnP step |
| • α - EI regularization parameter | |

2: **Initialize:** Neural network G_θ , $\mathbf{L}_0 = \mathbf{0}$, $\mathbf{u}_0 = \mathbf{0}$, $k = 0$;

3: **For** $i = 0, \dots, N - 1$ **do:**

4: **For** $y \in \mathcal{Y}$ **do:**

5: Sample T_g where $g \sim \mathcal{G}$;

6: Compute $x_0 = G_{\theta_k}(y)$, by default let $\mathbf{u}_k = x_0$;

7: Update $\mathbf{u}_{k+1} = \mathcal{D}[\mathbf{u}_k - \gamma[\nabla f_{\text{mc}}(y, A\mathbf{u}_k) + \lambda(\mathbf{u}_k - G_{\theta_k}(y) - \mathbf{L}_k^{(y)})]]$

8: Let $x_1 = \mathbf{u}_{k+1}$;

9: Transform $x_2 = T_g(x_1)$;

10: Compute $x_3 = G_{\theta_k}(Ax_2)$;

11: Update θ_{k+1} via progressively minimizing $\mathcal{L} = \mathbb{E}_{g \sim \mathcal{G}}\{\|x_0 + \mathbf{L}_k^{(y)} - x_1\|_2^2 + \alpha\|x_2 - x_3\|_2^2\}$ using an adaptive gradient-based optimizer (such as Adam) in each iteration;

12: Update $\mathbf{L}_{k+1}^{(y)} = \mathbf{L}_k^{(y)} - \tau(x_1 - G_{\theta_{k+1}}(y))$;

13: $k \leftarrow k + 1$

14: **End For**

15: **End For**

16: **Output:** G_{θ^*}

Algorithm 5 FEI with Equivariant Plug-and-Play (EQnP-PEI)

1: **Inputs:**

- \mathcal{Y} - Observations (training dataset)
- \mathbf{L} - Augmented Lagrangian multiplier
- λ - Augmented Lagrangian free parameter
- $\mathcal{D}(\cdot)$ - Denoiser
- α - EI regularization parameter
- N - number of epochs
- \mathcal{G} - Group of transformations
- \mathbf{u} - Initial gradient descent point of (18)
- γ - Gradient descent step size in PnP step

2: **Initialize:** Neural network G_θ , $\mathbf{L}_0 = \mathbf{0}$, $\mathbf{u}_0 = \mathbf{0}$, $k = 0$;

3: **For** $i = 0, \dots, N - 1$ **do:**

4: **For** $y \in \mathcal{Y}$ **do:**

5: Sample $T_g, T_{g'}$ where $g \sim \mathcal{G}, g' \sim \mathcal{G}$;

6: Compute $x_0 = G_{\theta_k}(y)$, by default let $\mathbf{u}_k = x_0$;

7: Update $\mathbf{u}_{k+1} = T_{g'}^{-1} \mathcal{D}[T_{g'}[\mathbf{u}_k - \gamma[\nabla f_{\text{mc}}(y, A\mathbf{u}_k) + \lambda(\mathbf{u}_k - G_{\theta_k}(y) - \mathbf{L}_k^{(y)})]]]$

8: Let $x_1 = \mathbf{u}_{k+1}$;

9: Transform $x_2 = T_g(x_1)$;

10: Compute $x_3 = G_{\theta_k}(Ax_2)$;

11: Update θ_{k+1} via progressively minimizing $\mathcal{L} = \mathbb{E}_{g \sim \mathcal{G}} \{ \|x_0 + \mathbf{L}_k^{(y)} - x_1\|_2^2 + \alpha \|x_2 - x_3\|_2^2 \}$ using an adaptive gradient-based optimizer (such as Adam) in each iteration;

12: Update $\mathbf{L}_{k+1}^{(y)} = \mathbf{L}_k^{(y)} - \tau(x_1 - G_{\theta_{k+1}}(y))$;

13: $k \leftarrow k + 1$

14: **End For**

15: **End For**

16: **Output:** G_{θ^*}

3. Numerical Experiments

This section describes the quantitative and qualitative experiments conducted to evaluate the performance of the proposed method.

Throughout the experiments, we compare our scheme (FEI) with (i) vanilla EI; (ii) PnP-FEI with a pre-trained denoiser, which in practice we consider DnCNN and BM3D. For these denoising algorithms, we choose the standard deviation of the noise as $\sigma = 1.0/\lambda$ (λ is the augmented Lagrangian parameter as presented in Algorithm 4) which are implemented via DeepInv toolbox¹. For a fair comparison with FEI, all the reported results for EI are obtained by directly running the released code of Chen et al. (2021). We use the same U-Net to build G_θ as suggested in Chen et al. (2021) for EI, FEI and PnP-FEI. Specifically, G_θ is a four-depth residual U-Net (Ronneberger et al., 2015) with a symmetric encoder-decoder and long skip connections. Each encoder comprises two 3×3 Convolution-BatchNorm-ReLU blocks with identity shortcuts, followed by 2×2 max pooling to double channels [64, 128, 256, 512]. The decoder mirrors the encoder in a refinement manner, and a final 1×1 convolution restores the output. For the measurement consistency loss, for simplicity, we choose ℓ_2 in this experiment.

1. <https://deepinv.github.io/deepinv/>

Framework	Optimization Backbone	Description
EI	Adam	Vanilla EI framework, which use back-propagation and end-to-end training strategy.
FEI-Option1	Adaptive HQS	HQS with accelerated gradient descent to approximately minimize Latent-reconstruction step subproblem, while Adam for online Pseudo-supervision, Algorithm 1.
FEI-Option2	Adaptive Linearized ADMM	The difference from FEI-Option1 is the change of splitting style to linearized ADMM, with gradient step for Latent-reconstruction, while Adam for online Pseudo-supervision, Algorithm 3.
PnP-FEI	Adaptive Linearized ADMM	The difference from FEI-Option2 is the use of pre-trained denoiser for Latent-reconstruction step instead of plain gradient step, Algorithm 4.
EQPnP-FEI	Adaptive Linearized ADMM	The difference from PnP-FEI is that we use equivariant plug-and-play to perform the Latent-reconstruction step, Algorithm 5.

Table 1: Unsupervised learning algorithms in our experiments.

3.1 Sparse-view CT

For the sparse-view CT task, when updating θ , we use Adam optimizer with an initial learning rate of 0.001 in all methods. The weight decay is 1×10^{-8} . We trained the networks for 10,000 epochs, keeping the learning rate constant for the first 5000 epochs, and then shrinking it by a factor of $0.5 \times (1 + \cos(\frac{\#epoch}{10000} \cdot \pi))$. We verify our model with equivariance strength $\alpha = 100$ as suggested in Chen et al. (2021). Other parameters of the FEI scheme are set as follows: Lagrangian multiplier $\lambda = 1$; NAG momentum factor $\beta = 0.1$; NAG step size $\eta = 0.01$; NAG iterations $J = 10$. The complete NAG algorithm is presented in Algorithm 2. The gradient descent step size in FEI-Option2 and PnP-FEI is $\gamma = 0.01$. We also use a moving average to smooth the reconstructed images for better reconstruction and smooth PSNR curves, the same as Sun et al. (2021).

The corresponding physics model A of sparse-view CT is the Radon transformation where 50 scans (angles) are uniformly subsampled to generate sparse-view sinograms (observations) y . The transformation we consider here is a group of rotations by randomly rotating 1 degree over 360 degrees. We use 10 images sampled (*index 1 to 10*) from the CT100 (Clark et al., 2013) dataset to train, and use another 10 images (*index 11 to 20*) with same number of scans to test the generalization performance of the networks trained by our methods. The image is resized to 128×128 (16384 pixels).

In order to better understand the boosts of proposed FEI scheme for sparse-view CT Imaging, we show the PSNR curves with respect to both iterations and times in Figure 1, and Table 2 shows the PSNR in the last iteration in Figure 1. In Figure 1 we can observe that the PnP-FEI is able to provide order-of-magnitude ($\geq 10\times$) acceleration over standard EI training.

We then test our methods with 50 Radon scan number (same as training) on another 10 images (*from index 11 to 20*), the results is reported in Table 3. We can observe that in terms of generalization performance,

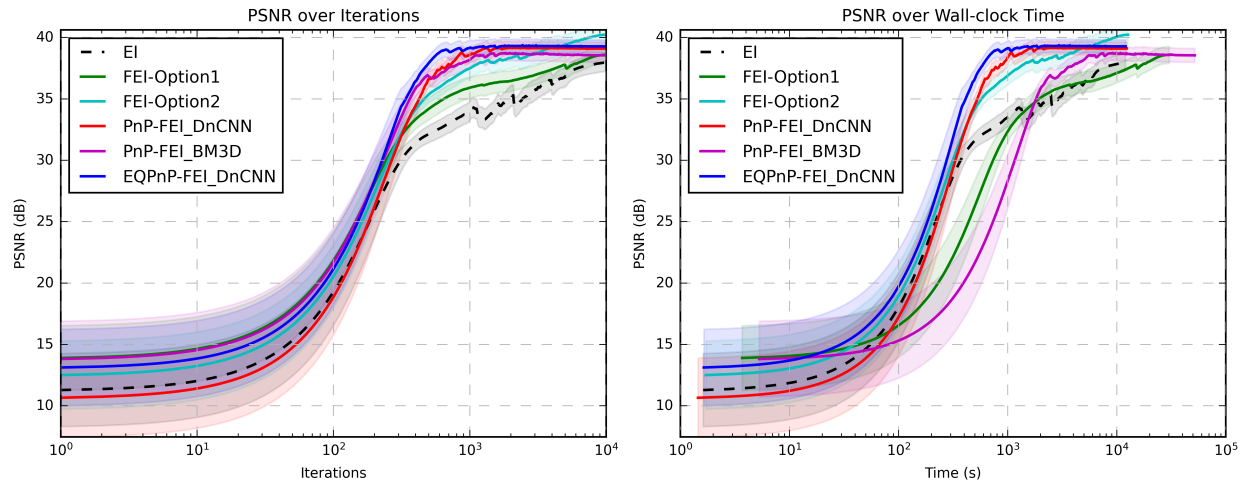


Figure 1: PSNR and MSE curves with respect to iteration during the training of Sparse-view CT reconstruction. We observe a 10-time acceleration can be achieved by PnP-FEI over EI (we fine-tuned EI with optimal algorithmic parameters for fastest convergence, but we did not fine-tune our own methods, so there is likely even more room for acceleration).

Methods	PSNR (dB)
*EI	37.98 ± 1.40
FEI-Option1	38.58 ± 1.34
FEI-Option2	40.22 ± 1.50
PnP-FEI (BM3D)	38.55 ± 1.08
PnP-FEI (DnCNN)	39.10 ± 1.00
EQPnP-FEI (DnCNN)	39.28 ± 1.02

Table 2: Averaged PSNR on training dataset at Figure 1 for Sparse-view CT reconstruction, * is baseline model.

the networks trained by our FEI/PnP-FEI both provide better generalization compared to the network trained by standard EI.

Methods	PSNR (dB)
FBP	27.98 ± 1.23
*EI	33.23 ± 1.55
FEI-Option1	33.93 ± 1.97
FEI-Option2	33.92 ± 1.77
PnP-FEI (BM3D)	33.95 ± 1.93
PnP-FEI (DnCNN)	34.06 ± 1.21
EQPnP-FEI (DnCNN)	34.12 ± 1.73
Supervised training	34.61 ± 2.12

Table 3: (Generalization performance) Averaged PSNR of 10 test images (*index 11 to 20*) for Sparse-view CT reconstruction, * is baseline model.

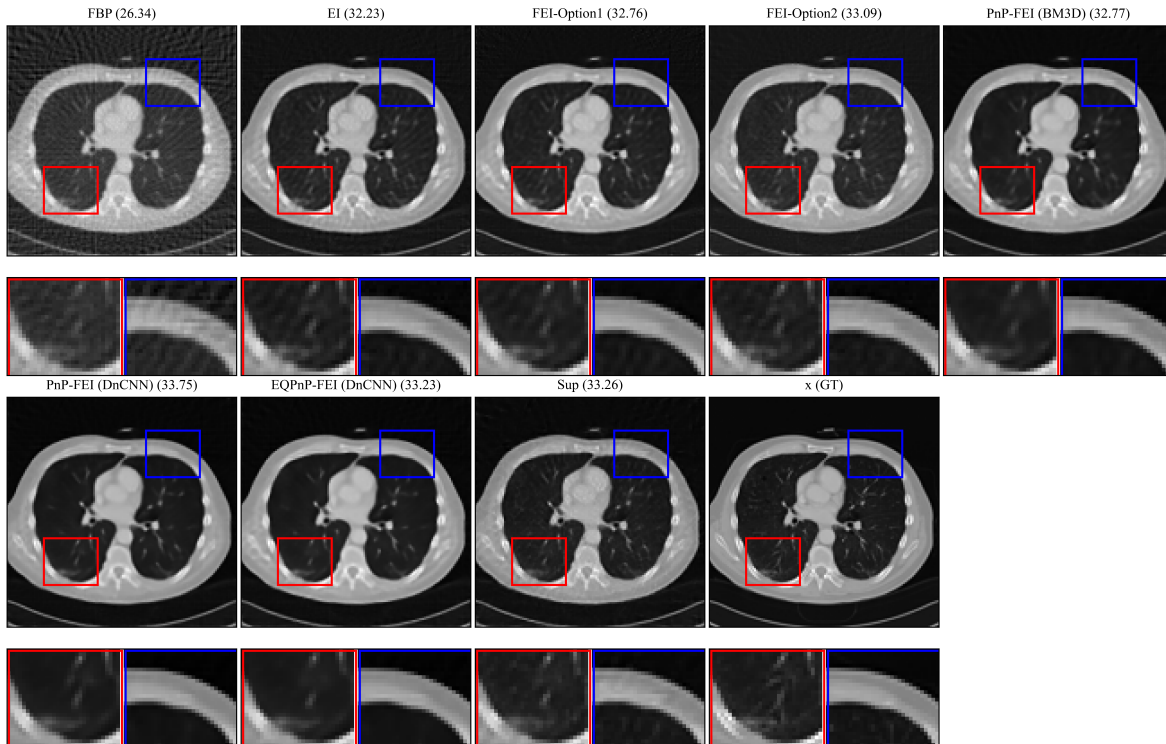


Figure 2: Test on another unseen CT100 sample with Radon scan number is 50.

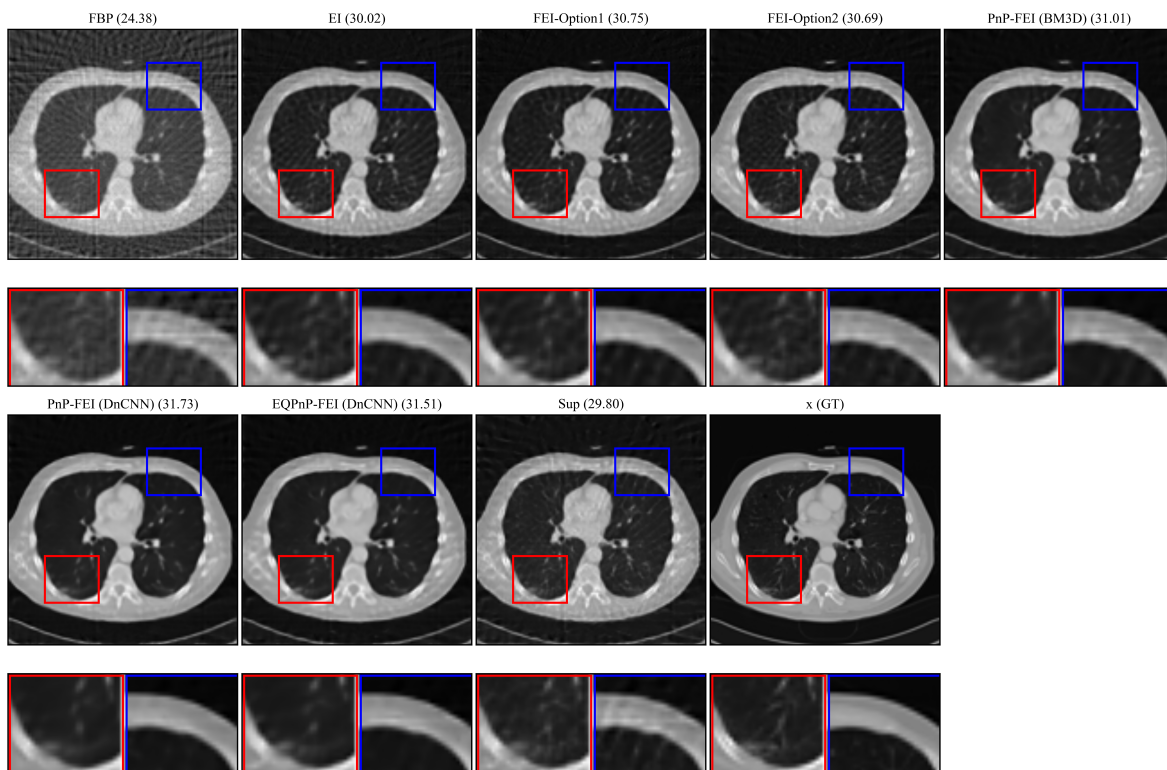


Figure 3: Test on unseen CT100 sample with Radon scan number is 40 (a test on out-of-distribution generalization).

3.2 Inpainting

For the inpainting task, when updating θ , we use the Adam optimizer with an initial learning rate of 0.001 in all methods. The weight decay is 1×10^{-8} . We trained the networks for 5,000 epochs, keeping the learning rate constant for the first 4,000 epochs, and then shrinking it by a factor of $0.5 \times (1 + \cos(\frac{\#epoch}{5000} \cdot \pi))$. We verify our model with equivariance strength $\alpha = 1$ as suggested in [Chen et al. \(2021\)](#). Other parameters of the FEI scheme are set as follows: Lagrangian multiplier $\lambda = 0.4$; NAG momentum factor $\beta = 0.9$; NAG step size $\eta = 0.09$; NAG iterations $J = 10$. The complete NAG algorithm is presented in [Algorithm 2](#). The size of the gradient descent step in FEI-Option2 and PnP-FEI is $\gamma = 1.0$. We also use a moving average to smooth the reconstructed images for better reconstruction and smooth PSNR curves, the same as [Sun et al. \(2021\)](#).

The mask rate for the inpainting task is 0.6, which means 60% of pixels are randomly removed. Here we choose random shift as the transformation. The dataset we used here is Urban100 ([Huang et al., 2015](#)) which is the same as [Chen et al. \(2021\)](#). For each image, we cropped a 512×512 pixel area in the center and then resized it to 256×256 for the ground truth image. The first 90 measurements are for training, while the last 10 images are for testing. We again observe significant benefit of FEI over standard EI training.

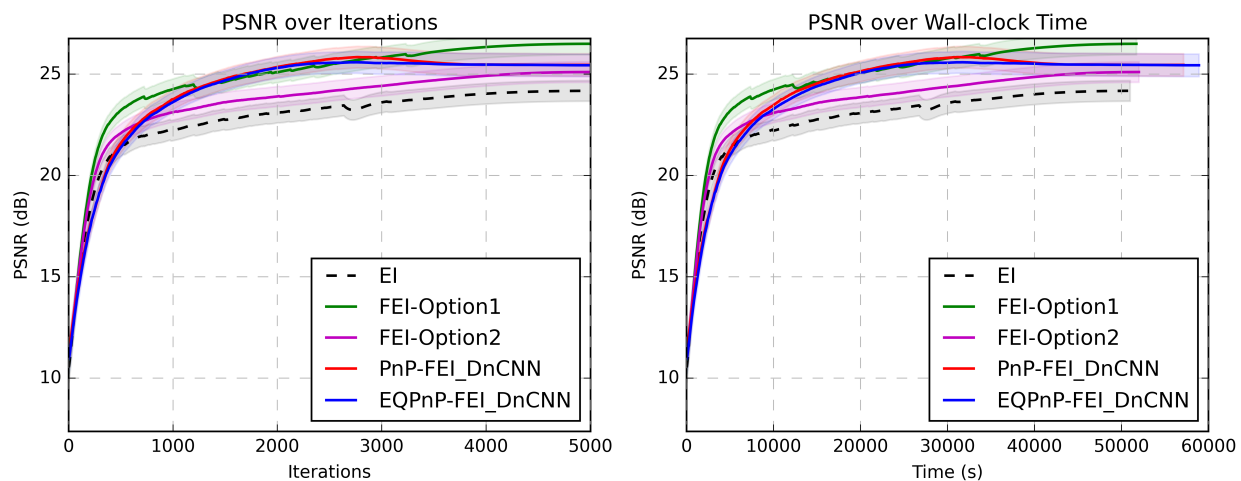


Figure 4: PSNR and MSE curves with respect to iteration during the training of inpainting reconstruction. We observe a significant acceleration can be achieved by FEI over EI (we fine-tuned EI with optimal algorithmic parameters for fastest convergence, but we did not fine-tune our own methods, so there is likely even more room for acceleration).

Methods	PSNR (dB)
*EI	24.18 ± 2.59
FEI-Option1	26.50 ± 2.74
FEI-Option2	25.11 ± 2.57
PnP-FEI (DnCNN)	25.46 ± 2.83
EQPnP-FEI (DnCNN)	25.44 ± 2.83

Table 4: PSNR on training dataset at [Figure 4](#) for inpainting reconstruction, * is baseline model.

Methods	PSNR (dB)
FBP	2.80 ± 1.66
*EI	21.19 ± 1.95
FEI-Option1	22.00 ± 2.10
FEI-Option2	21.51 ± 2.04
PnP-FEI (DnCNN)	21.39 ± 1.90
EQPnP-FEI (DnCNN)	21.81 ± 1.97
Supervised training	22.32 ± 2.30

Table 5: (Generalization performance) Averaged PSNR of 10 test images for inpainting reconstruction, * is baseline model.

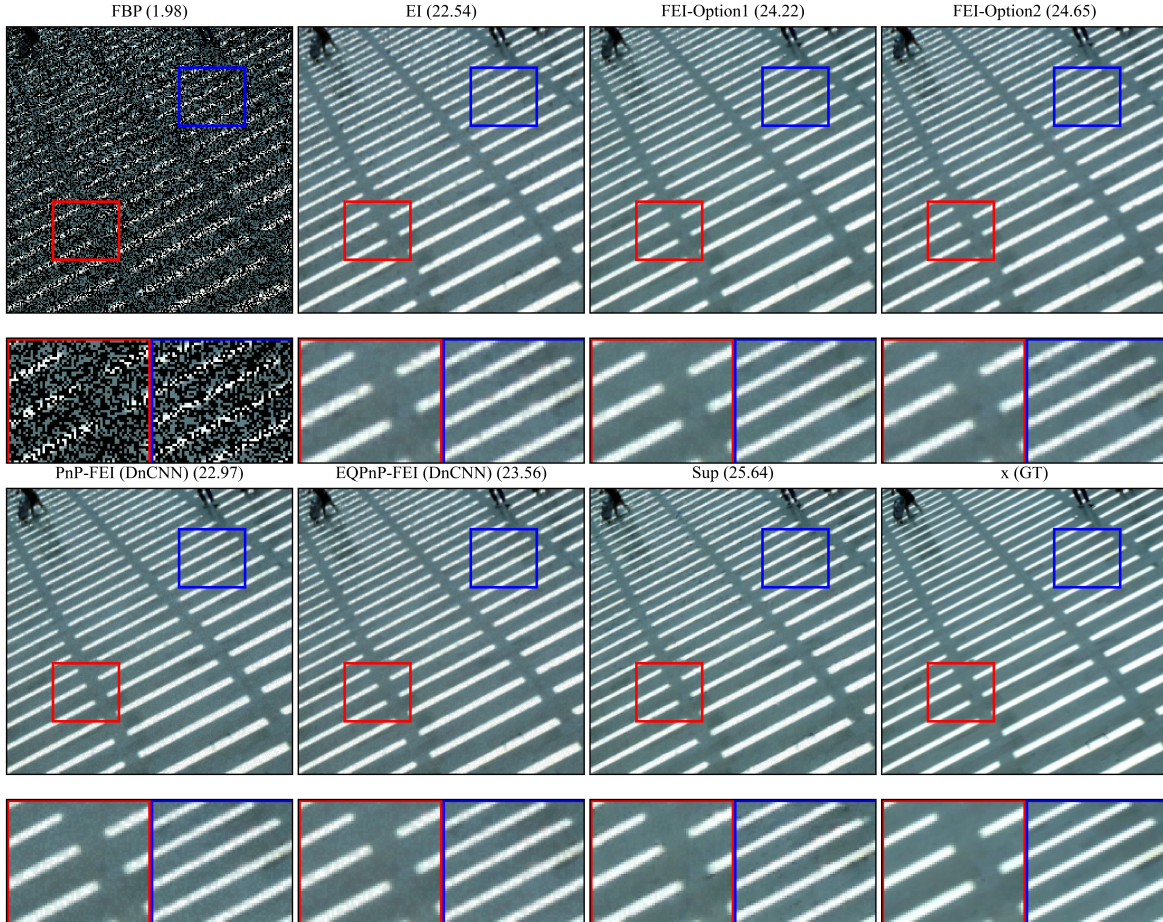


Figure 5: Test on another unseen Urban100 sample with mask rate is 0.6.

4. Conclusion

We propose FEI and its variant PnP-FEI for accelerating unsupervised training of deep neural networks to imaging inverse problems without the need of ground-truth data. We observe that our framework is capable of significantly accelerating the state-of-the-art unsupervised training scheme Equivariant Imaging proposed by (Chen et al., 2021), along with improved generalization performance. We believe that this work is crucial for the area of deep learning for computational imaging, via making the unsupervised training truly practical. Our algorithmic framework (Augmented Lagrangian plus PnP) can be easily extended to more recent variants of EI such as Robust Equivariant Imaging (REI) (Chen et al., 2022), Multi-Operator Imaging (MOI) (Tachella et al., 2022), and our Sketched Equivariant Imaging (SkEI) (Xu et al., 2024), etc.

References

- Manya V Afonso, José M Bioucas-Dias, and Mário AT Figueiredo. Fast image recovery using variable splitting and constrained optimization. *IEEE transactions on image processing*, 19(9):2345–2356, 2010.
- Dongdong Chen, Julián Tachella, and Mike E Davies. Equivariant imaging: Learning beyond the range space. In *Proceedings of the IEEE/CVF International Conference on Computer Vision*, pages 4379–4388, 2021.
- Dongdong Chen, Julián Tachella, and Mike E Davies. Robust equivariant imaging: a fully unsupervised framework for learning to image from noisy and partial measurements. In *Proceedings of the IEEE/CVF Conference on Computer Vision and Pattern Recognition*, pages 5647–5656, 2022.
- Kenneth Clark, Bruce Vendt, Kirk Smith, John Freymann, Justin Kirby, Paul Koppel, Stephen Moore, Stanley Phillips, David Maffitt, Michael Pringle, et al. The cancer imaging archive (tcia): maintaining and operating a public information repository. *Journal of digital imaging*, 26:1045–1057, 2013.
- K Dabov, A Foi, V Katkovnik, and K Egiazarian. Image denoising by sparse 3-d transform-domain collaborative filtering. *IEEE transactions on image processing: a publication of the IEEE Signal Processing Society*, 16(8):2080–2095, 2007.
- Derek Driggs, Junqi Tang, Jingwei Liang, Mike Davies, and Carola-Bibiane Schonlieb. A stochastic proximal alternating minimization for nonsmooth and nonconvex optimization. *SIAM Journal on Imaging Sciences*, 14(4):1932–1970, 2021.
- Matthias Joachim Ehrhardt, Zeljko Kereta, Jingwei Liang, and Junqi Tang. A guide to stochastic optimisation for large-scale inverse problems. *Inverse Problems*, 2025.
- Jia-Bin Huang, Abhishek Singh, and Narendra Ahuja. Single image super-resolution from transformed self-exemplars. In *Proceedings of the IEEE conference on computer vision and pattern recognition*, pages 5197–5206, 2015.
- Diederik P Kingma and Jimmy Ba. Adam: A method for stochastic optimization. *Proceedings of 3rd International Conference on Learning Representations*, 2015.
- Vishal Monga, Yuelong Li, and Yonina C Eldar. Algorithm unrolling: Interpretable, efficient deep learning for signal and image processing. *IEEE Signal Processing Magazine*, 38(2):18–44, 2021.

- Y. Nesterov. Gradient methods for minimizing composite objective function. Technical report, UCL, 2007.
- Yurii Nesterov. A method of solving a convex programming problem with convergence rate $o(1/k^2)$. In *Soviet Mathematics Doklady*, volume 27, pages 372–376, 1983.
- Olaf Ronneberger, Philipp Fischer, and Thomas Brox. U-net: Convolutional networks for biomedical image segmentation. In Nassir Navab, Joachim Hornegger, William M. Wells, and Alejandro F. Frangi, editors, *Medical Image Computing and Computer-Assisted Intervention – MICCAI 2015*, pages 234–241, Cham, 2015. Springer International Publishing. ISBN 978-3-319-24574-4.
- Zhaodong Sun, Fabian Latorre, Thomas Sanchez, and Volkan Cevher. A plug-and-play deep image prior. In *ICASSP 2021-2021 IEEE International Conference on Acoustics, Speech and Signal Processing (ICASSP)*, pages 8103–8107. IEEE, 2021.
- Julián Tachella, Dongdong Chen, and Mike Davies. Unsupervised learning from incomplete measurements for inverse problems. *Advances in Neural Information Processing Systems*, 35:4983–4995, 2022.
- Hong Ye Tan, Subhadip Mukherjee, Junqi Tang, and Carola-Bibiane Schönlieb. Provably convergent plug-and-play quasi-newton methods. *SIAM Journal on Imaging Sciences*, 17(2):785–819, 2024.
- Junqi Tang, Guixian Xu, Subhadip Mukherjee, and Carola-Bibiane Schönlieb. Practical operator sketching framework for accelerating iterative data-driven solutions in inverse problems. *hal-04820468*, 2024.
- Mathieu Terris, Thomas Moreau, Nelly Pustelnik, and Julian Tachella. Equivariant plug-and-play image reconstruction. In *Proceedings of the IEEE/CVF Conference on Computer Vision and Pattern Recognition*, pages 25255–25264, 2024.
- Singanallur V Venkatakrisnan, Charles A Bouman, and Brendt Wohlberg. Plug-and-play priors for model based reconstruction. In *2013 IEEE Global Conference on Signal and Information Processing*, pages 945–948. IEEE, 2013.
- Guixian Xu, Jinglai Li, and Junqi Tang. Sketched equivariant imaging regularization and deep internal learning for inverse problems. *arXiv preprint arXiv:2411.05771*, 2024.
- Kai Zhang, Wangmeng Zuo, Yunjin Chen, Deyu Meng, and Lei Zhang. Beyond a gaussian denoiser: Residual learning of deep cnn for image denoising. *IEEE Transactions on Image Processing*, 26(7):3142–3155, 2017.
- Qingping Zhou, Jiayu Qian, Junqi Tang, and Jinglai Li. Deep unrolling networks with recurrent momentum acceleration for nonlinear inverse problems. *Inverse Problems*, 40(5):055014, 2024.